PALEOCEANOGRAPHY, VOL. 24, PA2205, doi:10.1029/2008PA001653, 2009

Evidence for Indonesian Throughflow slowdown during Heinrich events 3–5

Rina Zuraida,[1,2] Ann Holbourn,[1] Dirk Nürnberg,[2] Wolfgang Kuhnt,[1]
Anke Dürkop,[1] and A. Erichsen[1]

Received 17 June 2008; revised 19 January 2009; accepted 6 February 2009; published 2 May 2009.

[1] We present sea surface and upper thermocline temperature records (60–100 year temporal resolution) spanning marine isotope stage 3 (~24–62 ka B.P.) from International Marine Global Change Study core MD01-2378 (121°47.27′E and 13°04.95′S; 1783 m water depth) located in the outflow area of the Indonesian Throughflow within the Timor Sea. Stable isotopes and Mg/Ca of the near-surface-dwelling planktonic foraminifer *Globigerinoides ruber* (white) and the upper thermocline–dwelling *Pulleniatina obliquiloculata* reveal rapid changes in the thermal structure of the upper ocean during Heinrich events. Thermocline warming and increased $\delta^{18}O_{seawater}$ (*P. obliquiloculata* record) during Heinrich events 3, 4, and 5 reflect weakening of the relatively cool and fresh thermocline flow and reduced export of less saline water from the North Pacific and Indonesian Seas to the tropical Indian Ocean. Three main factors influenced Indonesian Throughflow variability during marine isotope stage 3: (1) global slowdown in thermohaline circulation during Heinrich events triggered by Northern Hemisphere cooling, (2) increased freshwater export from the Java Sea into the Indonesian Throughflow controlled by rising sea level from ~60 to 47 ka, and (3) insolation-related changes in the Australasian monsoon with associated migration of hydrological fronts between Indian Ocean– and Indonesian Throughflow–derived water masses at ~46–40 ka.

Citation: Zuraida, R., A. Holbourn, D. Nürnberg, W. Kuhnt, A. Dürkop, and A. Erichsen (2009), Evidence for Indonesian Throughflow slowdown during Heinrich events 3–5, *Paleoceanography*, *24*, PA2205, doi:10.1029/2008PA001653.

1. Introduction

[2] Marine isotope stage 3 (MIS 3) is characterized by high-amplitude millennial-scale climate variability, which has been generally associated with shifts in ice sheet mass balance and changing modes of Atlantic meridional overturning circulation (AMOC) (see *Clark et al.* [2007] for detailed review). Greenland ice core and North Atlantic records revealed that abrupt episodes of warming of 8–16°C [*Huber et al.*, 2006] were followed by more gradual returns to colder (stadial) conditions. These climatic oscillations with a typical duration of 1 to 3 ka have become known as Dansgaard-Oeschger (D-O) events. Northern Hemisphere climate records also unmasked the occurrence of unusual layers of ice rafted debris, subsequently named Heinrich layers, which have been linked to episodic, massive discharges of icebergs released from the Laurentide ice sheet into the North Atlantic during extreme stadials.

[3] In contrast to Northern Hemisphere signals, climate variations appear to have been more subdued in the Southern Hemisphere with temperature changes of 1–3°C recorded in Antarctica during MIS 3 [*EPICA Community Members*, 2006]. Synchronization of Greenland and Antarctic ice cores using methane [*Blunier et al.*, 1998; *Blunier and Brook*, 2001; *EPICA Community Members*, 2006] additionally revealed that Southern Hemisphere climate fluctuations were clearly out of phase with Northern Hemisphere variations during this interval. In particular, episodes of greatest warming in Antarctica during MIS 3 (the so-called A1–A4 events) coincided with prolonged stadials or Heinrich events (HEs). However, the repercussion of this bipolar seesaw on Southern Hemisphere climate evolution is still unclear, in particular in the low latitudes to midlatitudes, since high-resolution climate proxy records are almost exclusively available from the Northern Hemisphere and southern high latitudes [*Lynch-Stieglitz*, 2004].

[4] Proxy data and ocean modeling results both indicated that millennial-scale climate variability was closely linked to changes in the rate of the AMOC. In particular, the AMOC is inferred to have considerably slowed down or even collapsed during HEs [*Sarnthein et al.*, 1994, 2001; *Alley and Clark*, 1999; *Ganopolski and Rahmstorf*, 2001; *Broecker*, 2003; *Piotrowski et al.*, 2004] resulting in major cooling at mid latitudes in the North Atlantic and southward displacement of the intertropical convergence zone (ITCZ). The widespread climatic impact of HEs was documented well beyond the North Atlantic in a variety of continental and marine settings including the Alboran Sea [*Cacho et al.*, 1999], Santa Barbara Basin [*Hendy and Kennett*, 2000], China [*Wang et al.*, 2001], Brazil [*Wang et al.*, 2004], Australia [*Muller et al.*, 2008], Borneo [*Partin et al.*, 2007] and the Indo Pacific region [*Dannenmann et al.*, 2003; *Levi et al.*, 2007]. The prevalence of a Northern Hemisphere climate signal at

[1]Institute of Geosciences, Christian Albrechts University, Kiel, Germany.
[2]Leibniz Institute of Marine Sciences at University of Kiel (IFM-GEOMAR), Kiel, Germany.

0883-8305/09/2008PA001653$12.00

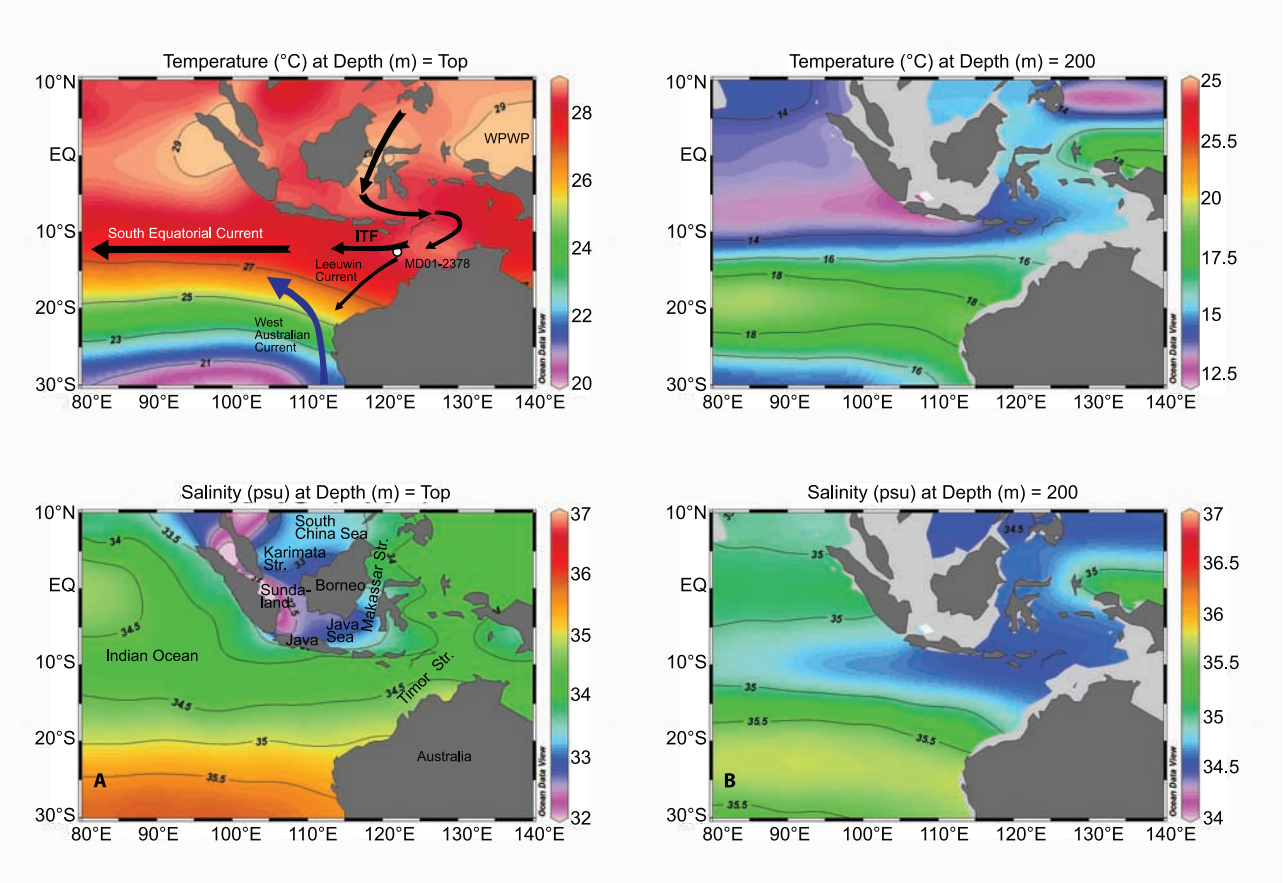

Figure 1. Annual temperature and salinity distribution in the Indo-Pacific region based on *World Ocean Atlas 2005* data [*Locarnini et al.*, 2006; *Antonov et al.*, 2006]. (a) Close to surface: habitat depth of *G. ruber* (white); (b) within upper thermocline: habitat depth of *P. obliquiloculata*. Arrows indicate modern current paths: ITF, South Equatorial Current, Leeuwin Current, and West Australian Current. Core MD01-2378 is located within the main ITF outflow (white circle).

locations far away from the North Atlantic was previously attributed to a tight coupling between regional climate systems through vigorous atmospheric teleconnections. In particular, changes in surface salinity within the Indo-Pacific region were interpreted as fundamental alterations in monsoonal regime related to southward shifts of the ITCZ during HEs.

[5] In contrast to the wealth of information concerning AMOC slowdown and related regional climatic impacts during HEs, relatively little is known about the effect of a reduction in North Atlantic deep water formation on the thermohaline circulation in the Pacific and Indian Oceans. The main return branch of the global thermohaline circulation consists of a westward flow from the Pacific Ocean through the Indonesian Archipelago where this flow is "transformed" to produce the Indonesian Throughflow (ITF). Changes in ITF volume and/or hydrographic properties significantly influence the temperature, salinity and nutrient distribution in the upper water column of the Indian Ocean with major repercussions for Australasian and African climate. The conversion of inflowing relatively cool and fresh North Pacific water through mixing and addition of freshwater within the archipelago into the ITF is modulated by seasonality and regional climate patterns [*Ilahude and Gordon*, 1996; *Sprintall et al.*, 2003]. The resulting ITF flows out of the Indonesian archipelago into the Indian Ocean through three eastern passages (Lombok, Ombai and Timor Straits). Among the three outflow passages, the Timor Strait plays the most significant role, in particular during times of lowered sea level, as it is substantially deeper and wider than the other two passages.

[6] We generated centennial resolution records of surface and upper thermocline $\delta^{18}O$ and Mg/Ca temperatures spanning MIS 3 (24–62 ka) in core MD01-2378 (13°4.95′S and 121°47.27′E; 1783 m water depth), situated within the main ITF outflow from the Timor Strait into the eastern Indian Ocean (Figure 1). Thus, this core is ideally located to monitor changes in ITF intensity and vertical structure and to resolve the impact of millennial-scale climate events on the ITF outflow and related effects on the tropical Indian Ocean. This work extends previous investigations of glacial-interglacial ITF variability in the same core [*Holbourn et al.*, 2005; *Xu et al.*, 2006, 2008] and in other cores located within the ITF outflow path [*Spooner et al.*, 2005; *Murgese and De Deckker*, 2007]. Our main objectives are (1) to detect the amplitude and frequency of changes in surface and

thermocline temperature and $\delta^{18}O$ within the main ITF outflow during MIS 3, (2) to test the hypothesis that a slowdown in thermohaline circulation during HEs reduces the cool and fresh ITF thermocline flow, and (3) to test modeling predictions that a reduction in ITF thermocline flow during HEs alters hydrographic profiles in the eastern Indian Ocean and leads to a warmer and saltier tropical Indian Ocean.

2. Methods

[7] This study is based on sediment samples (30–40 cc from 1 cm thick slices) taken at 1 cm interval (approximating 60–100 years) between 448 and 895 cm in International Marine Global Change Study core MD01-2378. Samples were initially dried and weighed, then washed over a 63 μm sieve. Residues were dried on a sheet of filter paper and weighed, then sieved into 63–150 μm, 150–250 μm, 250–315 μm, and >315 μm fractions. Coupled Mg/Ca and $\delta^{18}O$ analyses were performed on two species of planktonic foraminifer (*Globigerinoides ruber* (white sensu stricto) and *Pulleniatina obliquiloculata*) from the 250–315 μm size fraction to reconstruct surface and subsurface water masses conditions during MIS 3.

2.1. Mg/Ca Analysis

[8] Thirty well-preserved tests of the near-surface dweller *G. ruber* (white) and 20 tests of the thermocline dweller *P. obliquiloculata* were selected under a binocular microscope, then gently crushed between two glass plates and cleaned following the protocol outlined by *Barker et al.* [2003]. The choice of cleaning protocol was based on the relatively low terrigenous clay content in core MD01-2378 (carbonate content >70% [*Holbourn et al.*, 2005]). The first step (clay removal) involves rinsing foraminiferal fragments five times with ultrapure water, then twice with Aristar methanol, with ultrasonic treatment after each rinse. The next step is the removal of organic material using 250 μL of hot (97°C) oxidizing 1% $NaOH/H_2O_2$ reagent (10 mL 0.1 N analytical grade NaOH and 100 μL 30% suprapure H_2O_2) for 10 min. This process would produce gaseous buildup within sample tubes, therefore samples have to be agitated every 2.5 min to release bubbles. To maintain the chemical reaction, the samples were placed in an ultrasonic bath for a few seconds. The oxidizing solution was then removed by rinsing the samples three times with ultrapure water. The samples were then transferred into clean tubes and leached with 250 μL 0.001M HNO_3 (subboiled distilled) during a 30 s ultrasonic treatment, followed by two rinses with ultrapure water, in order to remove any adsorbed contaminant. The final step involves the dissolution of samples in 500 μL 0.075 M HNO_3 (subboiled distilled). The solution has to be diluted with ultrapure water to achieve Ca concentrations of 30–70 ppm.

[9] A total of 543 samples of *G. ruber* (white) and 596 of *P. obliquiloculata* were analyzed with the ICP-OES Spectro Ciros CCD SOP at the Institute of Geosciences, Christian-Albrechts-University, Kiel. The analytical error of the instrument is ~0.1%. The replicability of our measurements, based on 72 *G. ruber* (white) and 77 *P. obliquiloculata* replicate samples, is 0.2 mmol/mol (corresponding to 0.6°C) for *G. ruber* (white) and 0.2 mmol/mol (corresponding to 1°C) for *P. obliquiloculata*. We checked the validity of Mg/Ca values by evaluating the Fe/Mg contents of the samples using the limit of 0.1 mol/mol suggested by *Barker et al.* [2003]. As a result, one sample of *G. ruber* and one sample of *P. obliquiloculata* were rejected. The effect of dissolution on Mg/Ca in the interval 1–460 ka in core MD01-2378 was evaluated by *Xu et al.* [2006] using shell weights and a foraminiferal test fragmentation index. No significant effect of dissolution was detected even during the LGM and MIS 6, when dissolution would be most likely in the Timor Sea because of higher organic export flux [*Holbourn et al.*, 2005].

[10] Sea surface temperature (SST) and upper thermocline temperature were reconstructed from *G. ruber* (white) and *P. obliquiloculata* Mg/Ca values, respectively. Conversion of Mg/Ca values into temperature was performed using the general equation Mg/Ca = 0.38 (±0.02) exp 0.090 (±0.003)T for *G. ruber* (white) and the species specific Mg/Ca = 0.328 (±0.007) exp 0.090 (±0.003)T for *P. obliquiloculata* [*Anand et al.*, 2003]. The choice of equations was based on a study of 33 core tops [*Erichsen*, 2008] and 19 conductivity-temperature-depth (CTD) profiles taken during the Sonne 185 in October 2005 [*Kuhnt et al.*, 2006] and comparison to World Ocean Atlas (WOA) data [*Locarnini et al.*, 2006]. Mean *G. ruber* temperature (26.8°C with 0.82 standard deviation), estimated from the species specific equation of *Anand et al.* [2003], is significantly cooler than WOA annual average (28.3°C with 0.13 standard deviation) and CTD measurements at 10 m (27.6°C, with 0.42 standard deviation) from the Sonne 185 cruise. Mean SST (29.2°C with 0.93 standard deviation), based on the general equation of *Anand et al.* [2003], slightly overestimates WOA annual average by ~0.9°C, and agrees with mean WOA summer (January–March) SST (29.2°C with 0.25 standard deviation). Mean *P. obliquiloculata* temperature (23.7°C with 1.21 standard deviation), estimated from the species-specific equation, closely matches WOA annual average temperature at 100 m water depth (23.8°C with 0.49 standard deviation), and is only slightly warmer than CTD measurements at 100 m water depth (22.9°C with 1.44 standard deviation) from the Sonne 185 cruise. The choice of equations is additionally supported by calculation of calcification temperatures, based on $\delta^{18}O_{carbonate}$ and $\delta^{18}O_{seawater}$ measurements at five CTD stations. Mean calcification temperatures (28.6°C for *G. ruber* and 23.9°C for *P. obliquiloculata*) are close to WOA annual average values for sea surface (28.3°C) and 100 m water depth (23.8°C) and to our Mg/Ca-based estimates (29.2°C for *G. ruber* and 23.7°C for *P. obliquiloculata*). Core top Mg/Ca data and temperatures are provided in Table 1. Marine isotope stage 3 stable isotope, Mg/Ca and estimated temperature at MD01-2378 are archived at http://www.pangaea.de (doi:10.1594/pangaea.712515).

2.2. Stable Isotope Analysis

[11] For stable isotope analysis, we selected 20 tests of *P. obliquiloculata* from the 250–315 μm size fractions. All tests were checked for cement encrustations and infillings before being gently crushed between two glass plates and cleaned with methanol in an ultrasonic bath, then dried at

Table 1. Comparison of Average Water Temperatures at Sea Surface and 100 m Water Depth at 33 Stations in the Timor Sea With Mg/Ca-Derived Temperature Estimates From Equations of *Anand et al.* [2003] and With δ^{18}O-Derived Temperature Estimates[a]

	Minimum	Maximum	Stations	Mean	Median	SD	Variance	Standard Error
WOA05 annual mean SST	27.90	28.50	33	28.31	28.30	0.13	0.02	0.02
WOA05 austral summer (Jan–Mar) SST	28.80	29.50	33	29.16	29.20	0.25	0.06	0.04
WOA05 austral winter (Jul–Sep) SST	26.00	26.80	33	26.63	26.70	0.18	0.03	0.03
October 2005 SST from SO-185 CTD (at 10 m water depth)	26.80	28.40	19	27.65	27.60	0.42	0.18	0.10
Mg/Ca *G. ruber* (white) sensu stricto	4.25	6.62	33	5.27	5.20	0.45	0.20	0.08
Mg/Ca SST from general equation of *Anand et al.* [2003]	26.80	31.80	33	29.19	29.10	0.93	0.87	0.16
Mg/Ca SST from *G. ruber* (white) equation of *Anand et al.* [2003]	24.80	29.10	33	26.83	26.70	0.82	0.67	0.14
δ^{18}O *G. ruber*	−3.20	−2.30	32	−2.95	−3.00	0.19	0.04	0.03
G. ruber calcification temperature from δ^{18}O	25.90	29.70	32	28.60	28.80	0.79	0.62	0.14
WOA05 annual mean temperature at 100 m water depth	22.60	24.50	32	23.80	23.85	0.49	0.24	0.09
WOA05 austral summer (Jan–Mar) temperature at 100 m water depth	22.60	24.20	32	23.41	23.30	0.36	0.13	0.06
WOA05 austral winter (Jul–Sep) temperature at 100 m water depth	22.40	25.10	32	23.94	23.70	0.80	0.64	0.14
October 2005 temperature from CTD SO-185 CTD (at 100 m water depth)	18.40	24.60	18	22.94	23.35	1.44	2.07	0.34
Mg/Ca *P. obliquiloculata*	2.28	3.61	32	2.78	2.72	0.31	0.10	0.05
Mg/Ca *P. obliquiloculata* temperature from species specific equation of *Anand et al.* [2003]	21.50	26.70	32	23.69	23.50	1.21	1.46	0.21
Mg/Ca *P. obliquiloculata* temperature from *G. ruber* (white) equation of *Anand et al.* [2003]	18.60	23.20	32	20.55	20.40	1.07	1.15	0.19
δ^{18}O *P. obliquiloculata*	−2.10	−1.40	32	−1.83	−1.90	0.15	0.02	0.03
P. obliquiloculata calcification temperature from δ^{18}O	21.90	24.90	32	23.90	24.00	0.64	0.41	0.11

[a]CDT data are from the Sonne-185 cruise.

40°C. Measurements of 45 replicate samples indicate that the mean reproducibility is ±0.20‰ for δ^{18}O and ±0.12‰ for δ^{13}C. Stable isotope analysis was performed at IFM-GEOMAR on a Finnigan MAT 252 Mass Spectrometer with an automated Kiel carbonate preparation device. Samples were reacted by individual acid addition. The mean external error and reproducibility of carbonate standards is <0.07‰ for δ^{18}O and 0.07‰ for δ^{13}C. The values are reported relative to the Peedee Belemnite (PDB) scale, based on calibration to the National Bureau of Standards (NBS) 19. Stable isotope data for *G. ruber* (white) are from *Dürkop et al.* [2008].

2.3. Paleosalinity Reconstruction From $\delta^{18}O_{seawater}$

[12] Although reconstruction of paleosalinity from $\delta^{18}O_{seawater}$ ($\delta^{18}O_{sw}$) may have large error propagation, estimation from paired δ^{18}O and Mg/Ca analyses allows to narrow down the uncertainty limit [*Rohling*, 2007]. We calculated $\delta^{18}O_{sw}$ using the following equation $\delta^{18}O_{sw} = 0.27 + (T - 16.5 + 4.8 * \delta^{18}O) /4.8$ [*Bemis et al.*, 1998] for both *G. ruber* (white) and *P. obliquiloculata*. We used the *Orbulina universa* LL equation for both *G. ruber* and *P. obliquiloculata*, as the equation for the nonspinose *Globigerina bulloides* is only applicable for that species [*Bemis et al.*, 1998]. We additionally experimented with other equations (*O. universa* HL and *G. bulloides*), but found no significant differences in our results. Since the equation extracts the effect of temperature on oxygen isotope fractionation, the calculated $\delta^{18}O_{sw}$ is mainly influenced by $\delta^{18}O_{sw}$ variability related to continental ice volume and local $\delta^{18}O_{sw}$ fluctuations related to surface and upper thermocline salinities. In order to remove the ice volume effect and to test the robustness of our $\delta^{18}O_{sw}$ reconstructions, we used two different methods.

[13] 1. We applied one ice volume correction by subtracting benthic $\delta^{18}O_{sw}$ (five-point smoothed) from planktonic $\delta^{18}O_{sw}$ within the same samples. To calculate benthic $\delta^{18}O_{sw}$, we used the *Bemis et al.* [1998] equation, assuming bottom water temperature of 2°C and minimal fluctuations during MIS 3 [*Labeyrie et al.*, 1987]. The 2°C bottom water temperature assumption for MIS 3 is inferred from recent measurements of bottom temperature (2.8°C) at the location of core MD01-2378 during the Sonne 185 cruise [*Kuhnt et al.*, 2006]. This temperature difference is approximately half of that estimated between the Holocene and LGM [*Shackleton*, 1987].

[14] 2. We also applied an alternative ice volume correction based on the reconstructed MIS 3 sea level curve for the central Red Sea [*Siddall et al.*, 2003]. In order to ensure chronological compatibility, we tuned the Red Sea record to the MD01-2378 record. Then, we converted the sea level record into δ^{18}O units by assuming that a 1.1‰ change in δ^{18}O is equivalent to 130 m sea level change. Because of resolution difference (200 years in core KL11 and 60–100 years in core MD01-2378), we interpolated the rest of Red Sea δ^{18}O sea level values to fit the MD01-2378 age scale. Comparison between the two curves shows no significant differences in shape and absolute values, and supports that thermocline anomalies during MIS 3 are independent of the choice of ice volume correction.

2.4. Age Model

[15] The original age model for the MIS 3 interval in core MD01-2378 was derived from correlation of high-resolution

Table 2. Tie Points Between MD01-2378 Benthic Foraminiferal $\delta^{18}O$ and EDML Ice Core $\delta^{18}O$ and Between Planktonic Foraminifera $\delta^{18}O$ and NGRIP Ice Core $\delta^{18}O$[a]

Core MD01-2378		EDML Ice Core		
Depth (cm)	$\delta^{18}O$ (‰ Versus PDB)	GICC05 Age (ka B.P.)	$\delta^{18}O$ (‰ SMOW)	Event
342	3.92	18.15	−51.89	$\delta^{18}O$ maximum prior to deglaciation
506	3.92	27.45	−52.53	$\delta^{18}O$ maximum after AIM 4 event
554	3.72	30.65	−51.04	$\delta^{18}O$ maximum before AIM 4 event
642	3.31	38.15	−48.68	Last $\delta^{18}O$ minimum of A1 event
664	3.65	39.85	−50.91	$\delta^{18}O$ maximum before A1 event
742	3.28	47.25	−47.44	$\delta^{18}O$ minimum in center of A2 event
		NGRIP Ice Core		
Additional Tie Point	*G. ruber*	GICC05 Age (ka B.P.)	$\delta^{18}O$ (‰ SMOW)	Event
817	−1.58	54.49	−42.90	$\delta^{18}O$ maximum preceding D-O/14

[a]Tie points to EDML ice core are from *Dürkop et al.* [2008].

benthic oxygen isotope data to the isotope record of the EPICA Dronning Maud Land (EDML) ice core [*EPICA Community Members*, 2004], which was synchronized to the North Greenland Ice Core Project (NGRIP) ice core following the new Greenland Ice Core Chronology (GICC05) timescale [*EPICA Community Members*, 2006; *Andersen et al.*, 2006; *Svensson et al.*, 2006]. The MD01-2378 age model for this time interval is additionally constrained by 11 AMS ^{14}C dates, measured on *G. ruber* (white). Details of the original age model over the MIS 3 interval are provided by *Dürkop et al.* [2008, section 3.1, Figure 4]. In this study, we further constrained the MIS 3 interval between 742 and 895 cm with an additional tie point between the NGRIP oxygen isotope data on the GICC05 timescale [*Svensson et al.*, 2008] and our high-resolution planktonic $\delta^{18}O$ record. An interpolated curve was fitted through the tie points using a Stineman function, and it was used to determine the age of each sample. The lower part of our age model from 817 to 895 cm (corresponding to 54.5–62.5 ka) is based on linear extrapolation. Table 2 provides all tie points used in the revised age model for the MIS 3 interval in core MD01-2378.

3. Results

3.1. Oxygen Isotopes

[16] Planktonic foraminiferal $\delta^{18}O$ *G. ruber* (white) values vary between ∼−1.1‰ and −1.9‰ over the entire MIS 3 record (Figure 2). Three long-term trends are observed: (1) in the older part of the record before 55 ka, $\delta^{18}O$ values decrease from −1.5‰ to −1.9‰; (2) between 55 and 39 ka, planktonic $\delta^{18}O$ increases to −1.3‰; and (3) after a rapid decrease in planktonic $\delta^{18}O$ to −1.7‰ at 37.5 ka, a continuous increase of −0.6‰ occurs until 26 ka, followed by a slight decrease in values. Superimposed on this long-term variability are high-frequency variations, which show close affinity to fluctuations characteristic of northern high-latitude planktonic and ice core records. However, only the longer-lasting D-O warm events 8, 12, 14 and 16–17 are clearly expressed by decreases of ∼0.2‰ in the MD01-2378 record, whereas HEs 3–6 are marked by increases of ∼0.1–0.2‰ (Figure 2).

[17] The $\delta^{18}O$ *P. obliquiloculata* varies between 0.1 and −0.8‰, showing somewhat higher-amplitude variations than $\delta^{18}O$ *G. ruber* (white) (Figure 3). Three long-term trends are evident over the MIS 3 interval: (1) prior to 53.5 ka, $\delta^{18}O$ *P. obliquiloculata* values decrease from −0.2‰ to −0.7‰; (2) between 53 and 39 ka there is an overall increase from −0.7 to 0.0‰; and (3) following an initial decline to −0.3‰ at 39–38 ka, a long-term increase from −0.3 to 0.1‰ occurs between 38 and 24 ka. The $\delta^{18}O$ *P. obliquiloculata* curve is also characterized by high-frequency variations and the most pronounced D-O warm events 8, 12, 14 and 16–17 and the HEs 3–6 are detected by respective distinct increases and decreases of ∼0.1–0.2‰ (Figure 3).

3.2. Mg/Ca Temperature Reconstructions

[18] Average surface (25.6°C) and upper thermocline (21.0°C) Mg/Ca temperature estimates over MIS 3 in core MD01-2378 are cooler by nearly 3°C, compared to present-day mean annual SST of 28.3°C and upper thermocline temperature of 23.8°C (*World Ocean Atlas 2005* data [*Locarnini et al.*, 2006]). Figures 2 and 3 show that temperature oscillations are more pronounced within the thermocline water mass than at the surface: SST varies between 24.3°C and 27.0°C, whereas upper thermocline temperature varies between 18.8°C and 23.8°C.

[19] From 63 to 45 ka, SST values oscillate between 25 and 26°C. At 45–40 ka, the SST record is marked by a prominent cooling event, which corresponds to the interval between HE 4 and HE 5 and Antarctic warm events A1 and A2 (Figure 2). This major cooling event starts with a rather abrupt decrease of 1.5°C at the end of A 2 (46–45 ka), after which values oscillate around 25°C for a further ∼5 ka. The end of the cooling event is marked by a gradual warming of 1.5°C from ∼40 to 37 ka, after which SST are maintained around 25–26°C. In contrast to the thermocline temperature estimates, SST shows no clear imprint of HEs.

[20] Relatively high temperature values (centering around 22°C) are registered in the upper thermocline during HE 6 (Figure 3). From the end of HE 6, the upper thermocline record shows an overall cooling trend: from 22°C at 60 ka to 19.5°C at 48 ka, in contrast to the more consistent SST values. From 48 to 24 ka, temperatures fluctuate between 22°C and 20°C. However, a salient feature of the upper thermocline record within this interval is the occurrence of prominent increases in temperature during HEs 3–5, with lowest temperatures of ∼19.5°C at the beginning of each

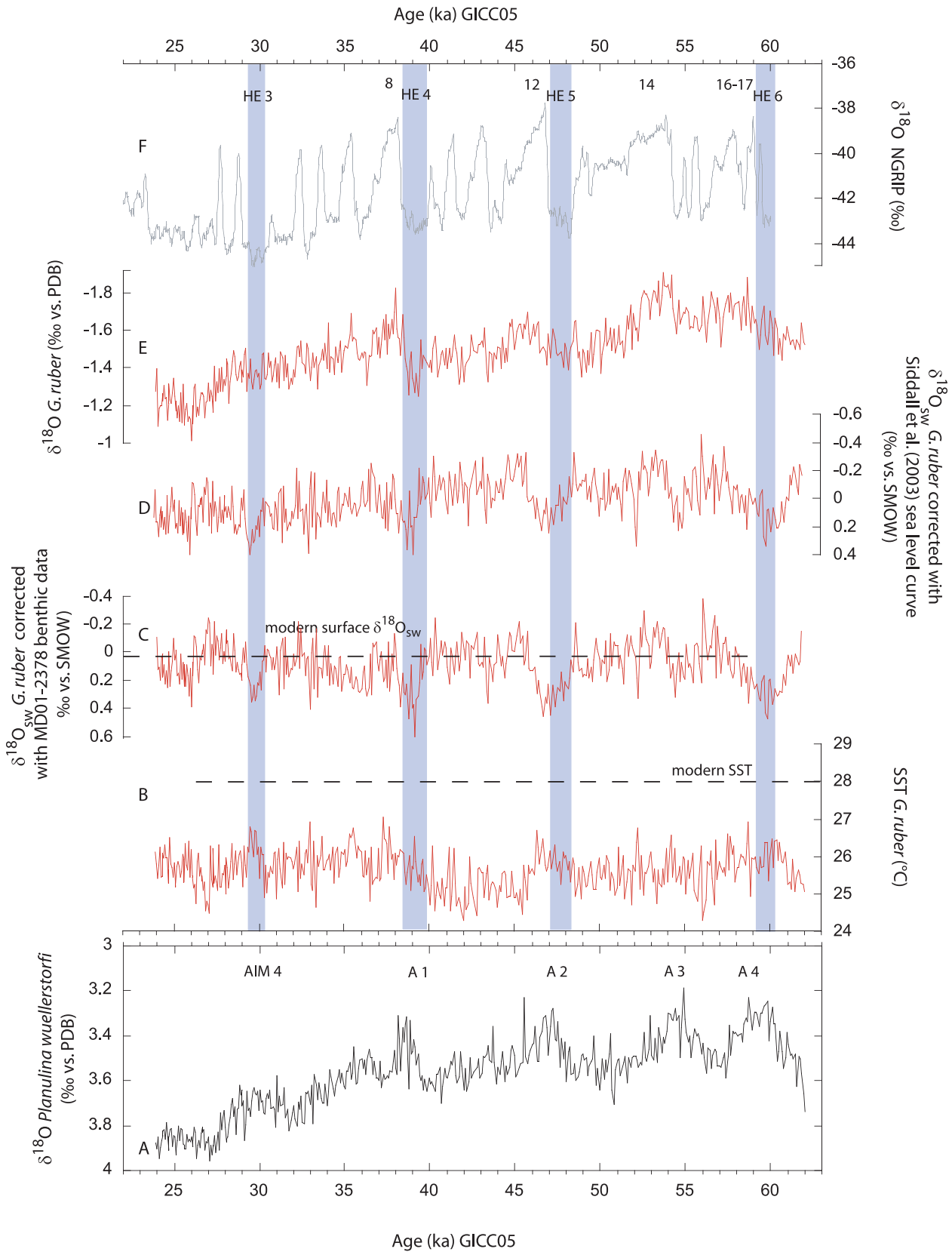
Age (ka) GICC05
HE 3
HE 4
HE 5
HE 6
8
12
14
16-17
F
E
D
C
B
A
δ18O NGRIP (‰)
δ18O G.ruber (‰ vs. PDB)
δ18O G.ruber corrected with Siddall et al. (2003) sea level curve (‰ vs. SMOW)
δ18Osw G.ruber corrected with MD01-2378 benthic data ‰ vs. SMOW)
modern surface δ18Osw
modern SST
SST G.ruber (°C)
AIM 4
A 1
A 2
A 3
A 4
δ18O Planulina wuellerstorfi (‰ vs. PDB)
Age (ka) GICC05

Figure 2

HE and peak temperatures in excess of 22–24°C at the end of each HE.

3.3. Sea Surface and Upper Thermocline Salinity Estimates ($\delta^{18}O_{sw}$)

[21] The MD01-2378 surface $\delta^{18}O_{sw}$ record (corrected for ice volume, see Methods) fluctuates between −0.3‰ and 0.4‰ SMOW with an average of 0.1‰ over MIS 3. Northern Hemisphere stadial events HEs 3–6 are marked by prominent increases of ∼0.2–0.3‰ in surface $\delta^{18}O_{sw}$ (Figure 2). HE 5 differs somewhat from other HEs, because high values (∼0.6–0.4‰) are maintained for ∼1 ka during the early part of this interstadial.

[22] Thermocline $\delta^{18}O_{sw}$ oscillates between −0.2‰ and 1.2‰ with an average of 0.4‰ over MIS 3. Values increase markedly by ∼0.2–0.4‰ (Figure 3) during HEs 3–6. The increase in thermocline $\delta^{18}O_{sw}$ during HE 5 is more gradual and less pronounced than during HEs 3–4. As for surface $\delta^{18}O_{sw}$, interstadials are generally characterized by values close to modern $\delta^{18}O_{sw}$.

[23] On the basis of measurements of water samples obtained during Sonne cruise 185, the modern values of surface $\delta^{18}O_{sw}$ and thermocline $\delta^{18}O_{sw}$ close to the position of our core are 0.05‰ and 0.20‰, respectively, which gives a difference of −0.15‰ between surface and thermocline. During MIS 3, the average difference between $\delta^{18}O_{sw}$ surface and thermocline water masses was −0.3‰, indicating a somewhat more stratified upper water column during MIS 3.

3.4. Carbon Isotopes

[24] Planktonic $\delta^{13}C$ of *G. ruber* (white) decreases between 64 and 60 ka during HE 6, reaching minimum value of ∼0.95‰ at 61 ka (Figure 4). From the end of HE 6, values show a two stepped, long-term increase: (1) from ∼1.2 to 1.5‰ between 60 and 52 ka and (2) from ∼1.4 to 1.6‰ between 52 and 31 ka. After 31 ka, values exhibit an overall decrease, reaching ∼1.3‰ at 23 ka. The $\delta^{13}C$ record of *P. obliquiloculata* also shows a decrease during HE 6: from ∼0.9 at 64 ka to ∼0.6‰ at 61 ka, after which values increase until ∼50 ka, when a maximum of ∼1.1‰ is attained. From 50 to 31 ka, values generally oscillate between ∼1.1 and 0.9‰. Between 31 and 23 ka, values show an overall decreasing trend from ∼1.1 to 0.9‰. As for the present day, the gradient between the *G. ruber* (white) and *P. obliquiloculata* $\delta^{13}C$ does not deviate markedly from 0.5‰ over the whole interval studied (Figure 4).

[25] Figure 4 shows that the *G. ruber* (white) and *P. obliquiloculata* $\delta^{13}C$ records exhibit overall similar trends as the epibenthic $\delta^{13}C$ in core MD01-2378. Comparison of surface, thermocline and bottom water $\delta^{13}C$ profiles in core MD01-2378 reveals an increasing trend from ∼60 to 50 ka, followed by a plateau until ∼30 ka and a final decrease until ∼23 ka. Comparison with Atlantic and Pacific records [*Pahnke and Zahn*, 2005; *Piotrowski et al.*, 2005] suggests that the increase at ∼60 to 50 ka is a global feature. Values ranging between ∼0.0 and 0.3‰ for benthic $\delta^{13}C$ are significantly lower than for planktonic $\delta^{13}C$, and are in agreement with present-day values at this location in the Timor Sea (Figure 5).

4. Discussion

4.1. Timor Sea Hydrography and Planktonic Foraminiferal Habitats

[26] The present-day upper thermal structure in the Timor Sea, close to the location of core MD01-2378, is characterized by a near-surface water mass (0–50 m water depth) with a relatively stable temperature averaging ∼28°C and a thermocline water mass (50–250 m water depth) exhibiting a steep temperature gradient from ∼28 to 12°C (Figure 5). Along with this marked temperature change, a sharp contrast in $\delta^{13}C$ also occurs within the upper water column (Figure 5) with values >1.2‰ in the upper 50 m declining to <1‰ at ∼100 m and reaching ∼0.4–0.1‰ below 250 m. The temperature difference between surface and upper thermocline (∼100 m water depth) water masses is ∼5°C today, which compares well with the range of values registered during MIS 3 (Figures 2 and 3), suggesting that our temperature reconstructions provide realistic estimates, although thermocline temperature appears to have fluctuated more than SST during MIS 3. The planktonic and benthic $\delta^{13}C$ profiles over MIS 3 also show broad agreement with modern $\delta^{13}C$ values for surface, thermocline and bottom water masses, even though long- and short-term temporal variations are detected within the three records (Figure 4).

[27] One of the limitations in the application of multispecies Mg/Ca thermometry is that interspecies differences may reflect the migration of some species within the water column during their life cycle and/or changes in habitat depth rather than real temperature changes at a constant depth. The near-surface dweller *G. ruber* (white) exhibits relatively consistent Mg/Ca values [*Eggins et al.*, 2003] indicating that the effect due to vertical migration is negligible and calculated SST accurately reflect the assigned habitat depth of upper 50 m for this species [*Anand et al.*, 2003]. In terms of seasonality, *G. ruber* (white) Mg/Ca commonly reflects average annual hydrographic conditions because of the almost uniform occurrence of this species throughout the year [*Hemleben et al.*, 1989; *Lin et al.*, 1997; *Tedesco and Thunell*, 2003]. However, in the Timor Sea, core top values of *G. ruber* fall into the range of average summer SST (29°C) [*Xu et al.*, 2006, Table 1]. Although the deeper dweller *P. obliquiloculata* exhibits high mobility in the water

Figure 2. (a) Benthic $\delta^{18}O$ (*P. wuellerstorfi*) spanning MIS 3 in core MD01-2378 from *Dürkop et al.* [2008]. AIM 4 and A1–A4 refer to Antarctic warm events. (b) *G. ruber* (white) Mg/Ca-derived SST; average SST over MIS 3 is 25.6°C, in contrast to present-day annual SST of 28.3°C [*Locarnini et al.*, 2006]. (c) Surface $\delta^{18}O_{sw}$; note that dashed line indicates modern surface $\delta^{18}O_{sw}$ measured in water samples from the SO-185 cruise (0.05‰). (d) Surface $\delta^{18}O_{sw}$ corrected with the Red Sea ice volume curve of *Siddall et al.* [2003]. (e) Planktonic $\delta^{18}O$ of *G. ruber* (white) from *Dürkop et al.* [2008]. (f) NGRIP ice core $\delta^{18}O$ plotted on the common GICC05 timescale [*Svensson et al.*, 2006, 2008]. Numbers refer to longer-lasting D-O events. Shaded bars indicate Heinrich events (HEs 3–6).

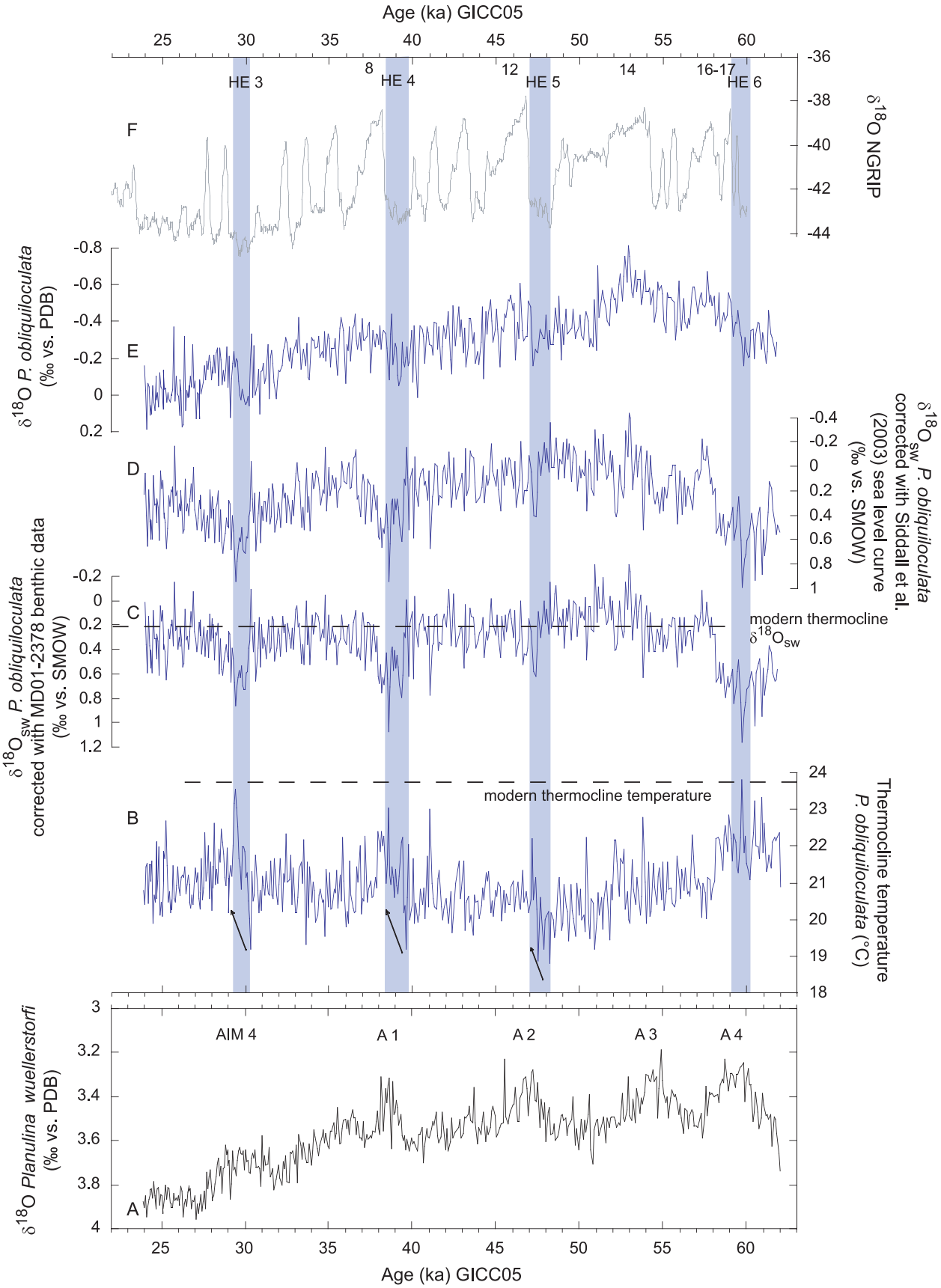
Age (ka) GICC05
HE 3
HE 4
HE 5
HE 6
8
12
14
16-17
F
δ18O NGRIP
E
δ18O P. obliquiloculata (‰ vs. PDB)
D
δ18Osw P. obliquiloculata corrected with Siddall et al. (2003) sea level curve (‰ vs. SMOW)
C
δ18Osw P. obliquiloculata corrected with MD01-2378 benthic data (‰ vs. SMOW)
modern thermocline δ18Osw
B
modern thermocline temperature
Thermocline temperature P. obliquiloculata (°C)
A
δ18O Planulina wuellerstorfi (‰ vs. PDB)
AIM 4
A 1
A 2
A 3
A 4
Age (ka) GICC05

Figure 3

column and seasonality [*Prell and Damuth*, 1978], sediment trap studies indicate that this species mainly calcifies below the mixed layer [*Bé*, 1977; *Ravelo et al.*, 1990; *Pflaumann and Jian*, 1999] or between 50 and 100 m [*Anand et al.*, 2003]. *Ravelo and Fairbanks* [1992] and *Cléroux et al.* [2007] also inferred *P. obliquiloculata* living within the seasonal thermocline, which in the Timor Sea is between 50 and 250 m (CTD data from SO-185 cruise).

[28] Several lines of evidence also support that temperature estimates derived from *P. obliquiloculata* in core MD01-2378 do not relate to changes in habitat depth but to temperature variations occurring within the upper thermocline. First, a comparison of CTD temperature profiles from the Timor Sea with temperature estimates of *P. obliquiloculata* from 33 Timor Sea core tops confirms that an estimated habitat depth below 100 m for *P. obliquiloculata* is reasonable for the present day in this area (Table 1). Second, the overall δ^{13}C gradient between *G. ruber* (white) and *P. obliquiloculata* does not deviate substantially from ~0.5‰ throughout MIS 3 (Figure 4), supporting that the respective habitat depths of *P. obliquiloculata* and *G. ruber* (white) remained overall quite consistent over this extended interval. Finally, δ^{13}C and temperature do not covary during MIS 3, which would be expected if *P. obliquiloculata* migrated through the upper water column and thus reflected ambient temperature and δ^{13}C gradients. For instance, temperature increases during HEs coincide with no significant change or even with slight decreases in δ^{13}C (Figures 3 and 4).

4.2. Decrease in ITF Intensity During Heinrich Events

[29] A striking feature of the Timor Sea record over MIS 3 is the contrast between the benthic and planktonic oxygen isotope signals (Figures 2 and 3). Whereas benthic δ^{18}O captures Antarctic warming and cooling trends including the AIM 4 and A1 to A4 warm events, planktonic δ^{18}O shows closer similarity to Northern Hemisphere records [*Dürkop et al.*, 2008]. For instance, increases in δ^{18}O *G. ruber* (white) of ~0.1–0.2 ‰ are registered during stadials HEs 3–6, which also correspond to the early phases of warming in Southern Hemisphere A1–A4 events. This distinct out of phase relationship between benthic and planktonic δ^{18}O events was previously interpreted as a bipolar climate seesaw, as Northern Hemisphere cooling/warming is balanced by Southern Hemisphere warming/cooling [*Broecker*, 1998; *Shackleton et al.*, 2000].

[30] However, our SST record indicates little change during stadials and interstadials, implying that δ^{18}O *G. ruber* (white) maxima during HEs 3–6 are mainly due to $\delta^{18}O_{sw}$ increases, as shown in Figure 2. Tropical records from the West Pacific Warm Pool region also revealed that stadials were characterized by heavier $\delta^{18}O_{sw}$ in surface-dwelling foraminifers. These $\delta^{18}O_{sw}$ increases were interpreted as a shift toward cooler and drier (El Nino-like) conditions during stadials [*Stott et al.*, 2002; *Dannenmann et al.*, 2003; *Rosenthal et al.*, 2003; *Levi et al.*, 2007]. However, the Timor Sea record from core MD01-2378 additionally displays prominent increases in thermocline temperature and $\delta^{18}O_{sw}$ during HEs 3–6 (Figures 2 and 3). We attribute these changes to an increased influence of warmer, saltier thermocline water from the tropical Indian Ocean and a concurrent decrease in cool, fresh ITF thermocline flow, due to an overall slowdown in the global thermohaline circulation during HEs. The decreased freshwater export from the North Pacific would additionally contribute to higher salinity ($\delta^{18}O_{sw}$) in the tropical eastern Indian Ocean.

[31] Proxy data and ocean model simulations indicate a near collapse of the MOC during HEs [*Sarnthein et al.*, 1994, 2001; *Alley and Clark*, 1999; *Ganopolski and Rahmstorf*, 2001; *Broecker*, 2003; *Piotrowski et al.*, 2004]. Model experiments also predict that a slowdown in the global thermohaline circulation (for instance during the LGM) would result in a weaker ITF, which in turn would diminish the southward flowing Leeuwin Current and the fresh and cool thermocline flow feeding the South Equatorial Current [*De Deckker et al.*, 2003; *Gordon*, 2005]. Today, the southern front of the cool and fresh thermocline water mass, which is injected into the eastern equatorial Indian Ocean by the ITF, is located at approximately 13–14°S [*Gordon*, 2005; *Locarnini et al.*, 2006; *Antonov et al.*, 2006], close to the position of core MD01-2378. During periods of reduced thermohaline circulation and weakened ITF flow, this front might have moved northward. Thus, the location of core MD01-2378 became increasingly influenced by relatively warm, salty thermocline water from the Indian Ocean rather than by cooler, fresher thermocline water flowing out of the Indonesian seas into the Timor Sea.

[32] The pace and amplitude of thermocline warming and $\delta^{18}O_{sw}$ changes differed significantly during successive HEs. The most sustained episode of ITF weakening and thermohaline slowdown occurred at the end of MIS 4 and through HE 6, as indicated by highest temperature and $\delta^{18}O_{sw}$ values persisting over ~3 ka (Figure 3). Sharp drops in thermocline temperature and $\delta^{18}O_{sw}$ occurred only at ~58.5 ka, which is ~1 ka later than the end of HE 6. The early part of HE 5 was characterized by minimum thermocline temperature values and low $\delta^{18}O_{sw}$, marking the end of a long-term increase in ITF intensity from ~60 to 47 ka before a sharp decrease in ITF flow toward the end of HE 5. HEs 3–4 also coincided with prominent decreases in ITF

Figure 3. (a) Benthic δ^{18}O (*P. wuellerstorfi*) spanning MIS 3 in core MD01-2378 from *Dürkop et al.* [2008]. AIM 4 and A1–A4 refer to Antarctic warm events. (b) *P. obliquiloculata* Mg/Ca-derived upper thermocline temperature (100 m water depth); average value over MIS 3 is 21°C, in contrast to present-day annual value of 23.8°C [*Locarnini et al.*, 2006]. (c) Upper thermocline $\delta^{18}O_{sw}$; note that dashed line indicates modern upper thermocline $\delta^{18}O_{sw}$ measured in water samples from the SO-185 cruise (0.20‰). (d) Thermocline $\delta^{18}O_{sw}$ corrected with the Red Sea ice volume curve of *Siddall et al.* [2003]. (e) Planktonic δ^{18}O of *P. obliquiloculata*. (f) NGRIP ice core δ^{18}O plotted on the common GICC05 timescale [*Svensson et al.*, 2006, 2008]. Numbers refer to longer-lasting D-O events. Shaded bars indicate Heinrich events (HEs 3–6). Arrows highlight temperature changes during HEs.

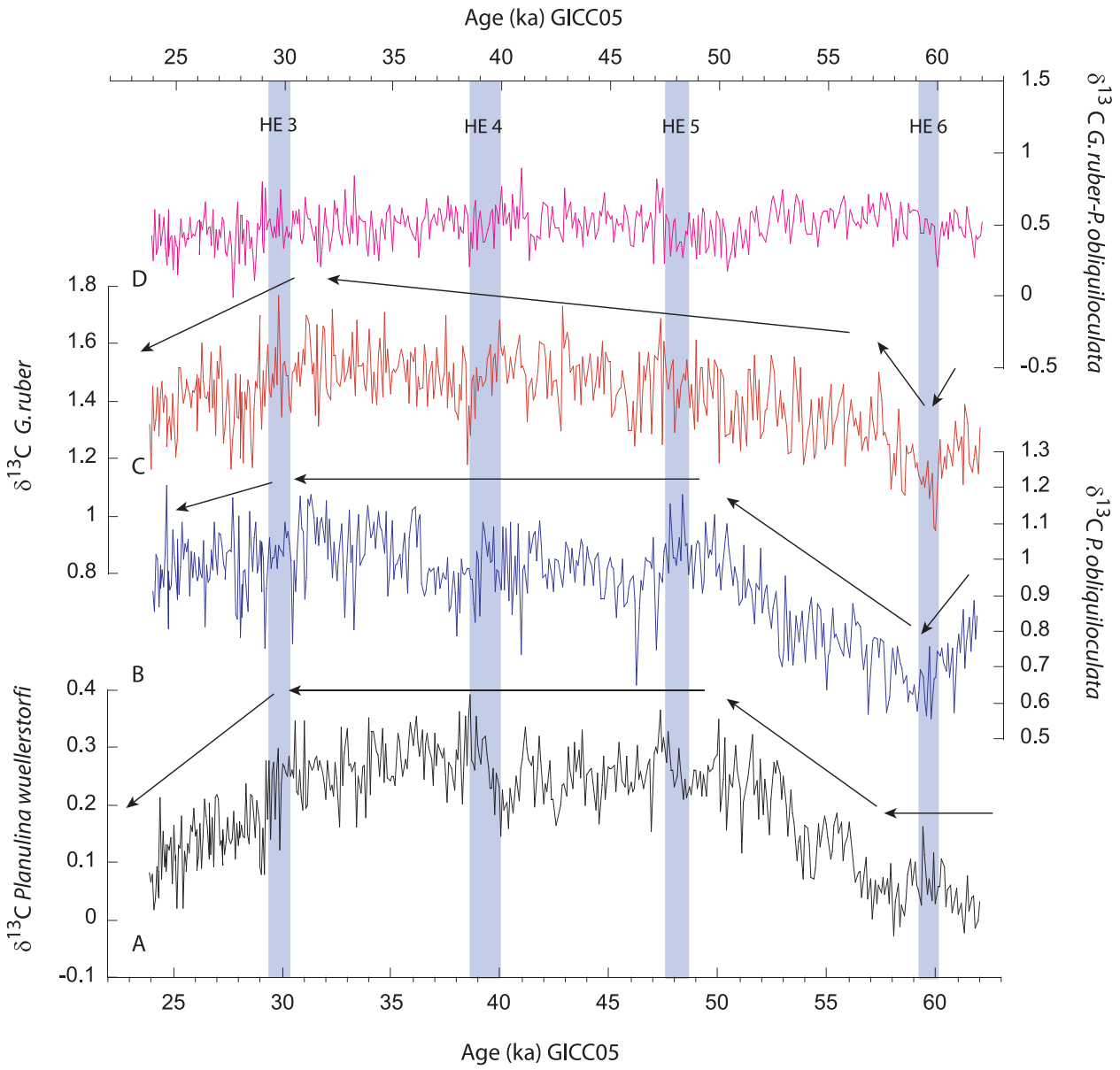

Figure 4. (a) Benthic δ^{13}C (*P. wuellerstorfi*) spanning MIS 3 in core MD01-2378 from *Dürkop et al.* [2008]. (b) Planktonic δ^{13}C of upper thermocline dweller *P. obliquiloculata*. (c) Planktonic δ^{13}C of near-surface dweller *G. ruber* from *Dürkop et al.* [2008]. (d) Consistent δ^{13}C gradient between *G. ruber* and *P. obliquiloculata* supports that respective depth habitats of these two species did not change significantly during MIS 3. Arrows highlight main trends during MIS 3.

flow, however the declines in ITF intensity occurred more gradually over these stadial events. For HE 4, the decrease in ITF flow was maintained for a few hundred years after the end of the stadial, which is not surprising, as HE 4 is considered the most intense of the six Heinrich layers in the North Atlantic [*Hemming*, 2004].

4.3. Main Controls of ITF Variability During MIS 3

[33] Global changes in thermohaline circulation evidently exert a major control on ITF variability, as demonstrated by the prominent decreases in outflow intensity registered during HEs 3–6. However, the different expression of HEs as well as the longer trends of ITF variability detected in our Timor Sea record suggest that the strength of the thermohaline circulation is not the sole control on ITF intensity and that additional factors may also play a significant role. Today, links between wind surges from the South China Sea prior to and during the onset of the Australian monsoon provide evidence for cross-equatorial atmospheric connections between the Asian winter monsoon and Australian summer monsoon [*Suppiah and Wu*, 1998]. During MIS 3, such cross-equatorial connections would have effectively linked ITF

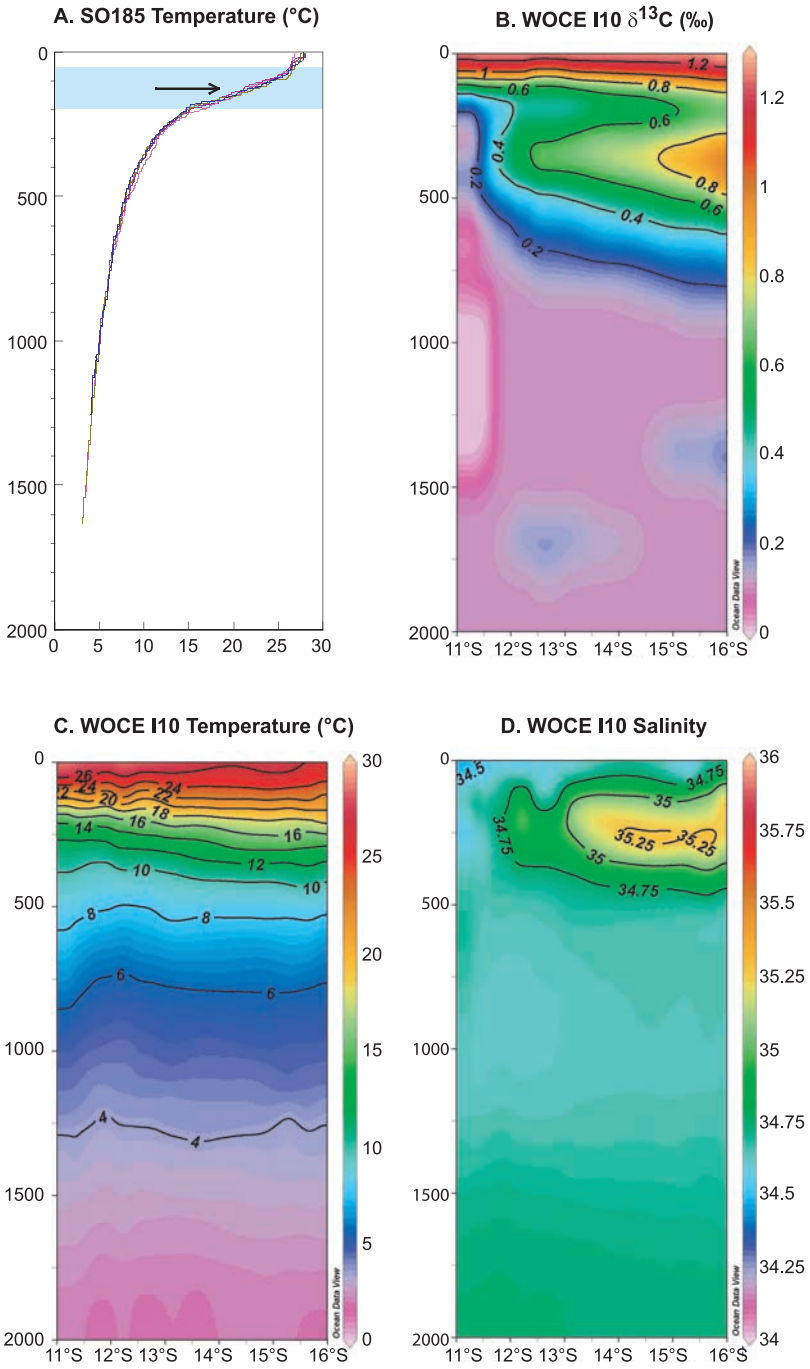

Figure 5. (a) Timor Sea temperature profiles obtained in September 2005 during the SO-185 cruise [*Kuhnt et al.*, 2006] indicate temperature difference of ~5°C between surface and upper thermocline. Shaded bar indicates the extent of the thermocline with an arrow at the base of the upper thermocline, where *P. obliquiloculata* calcifies [*Ravelo and Fairbanks*, 1992; *Cléroux et al.*, 2007]. (b) Temperature profile along World Ocean Circulation Experiment (WOCE) line i10 (plotted section starts from South Java). (c) The δ^{13}C profile along WOCE line i10. (d) Salinity profile along WOCE line i10. WOCE data are available at http://doi.pangaea.de/10.1594/PANGAEA.277652.

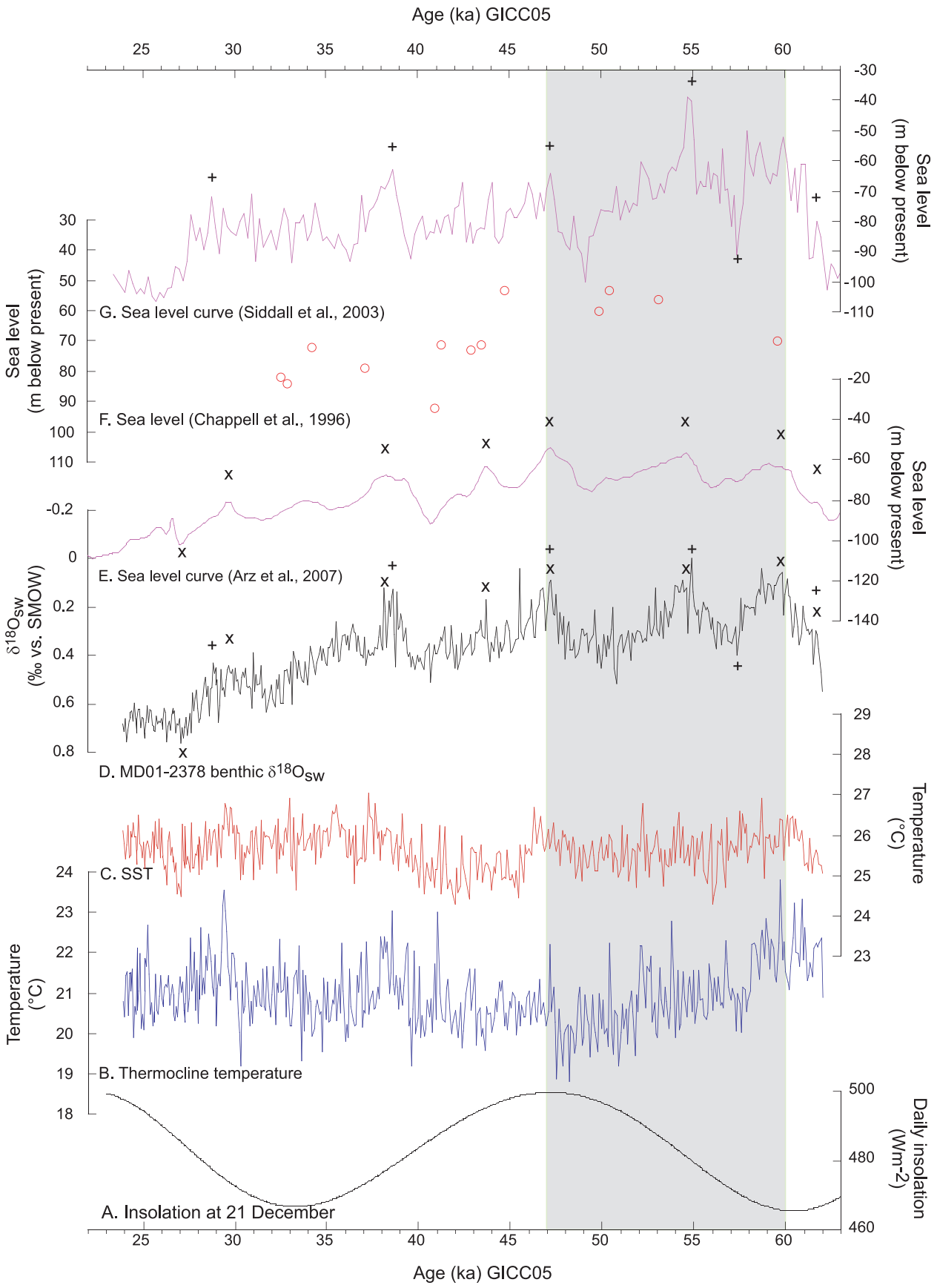
Age (ka) GICC05
25 30 35 40 45 50 55 60
G. Sea level curve (Siddall et al., 2003)
Sea level (m below present)
30 40 50 60 70 80 90 100 110
-30 -40 -50 -60 -70 -80 -90 -100 -110
F. Sea level (Chappell et al., 1996)
-20 -40 -60 -80 -100 -120 -140
E. Sea level curve (Arz et al., 2007)
δ18Osw (‰ vs. SMOW)
-0.2 0 0.2 0.4 0.6 0.8
D. MD01-2378 benthic δ18Osw
C. SST
Temperature (°C)
29 28 27 26 25 24 23
B. Thermocline temperature
24 23 22 21 20 19 18
A. Insolation at 21 December
Daily insolation (Wm-2)
500 480 460

Figure 6

outflow intensity to rapid, large-amplitude climate events in the Northern Hemisphere high latitudes. Intensification of the Australian monsoon triggered by episodes of Northern Hemisphere cooling would have piled up water masses in the eastern Indian Ocean, thus decreasing further the ITF outflow into the Timor Sea during HEs.

[34] A unique feature of the ITF is the en route alteration of inflowing Pacific water into a strongly stratified thermocline dominated flow at the southern end of the Makassar Strait [*Gordon*, 2005]. This change in ITF vertical structure is dependent on sea level and the strength of the SE Asian boreal winter monsoon. Today, thermocline flow of relatively cool water dominates during boreal winter, as the warm surface flow becomes blocked by the development of a fresh water plug at the southern tip of the Makassar Strait, driven by monsoonal winds from the South China Sea through the Java Sea [*Gordon et al.*, 2003]. As a result, the ITF becomes cooler, fresher, and dominated by thermocline rather than surface flow [*Gordon et al.*, 2003]. However, this mechanism requires an open marine connection between the South China and Java Seas over a flooded Sunda shelf, which relates to a sea level position of at least 80 m above the LGM sea level, equivalent to the present-day sill depth of the Karimata Strait (~40 m).

[35] Comparison of sea level reconstructions for MIS 3 indicates that this threshold was not reached during MIS 4, most of MIS 3 and the LGM (Figure 6). However, significant freshwater input may have occurred from Java, Borneo and Sundaland into the Java Sea, which increasingly became submerged at times of rising sea level during MIS 3. The most recent sea level curves [*Siddall et al.*, 2003; *Arz et al.*, 2007] indicate that the shelf of the Java Sea became flooded in the early part of MIS 3 (after ~60 ka), as sea level reached 60–70 m below present-day level. The long-term increasing trend of thermocline cooling from 60 to 47 ka (Figure 3) may have been driven by the establishment of the Java Sea freshwater export, as sea level rose following the MIS 4 lowstand. Intensified SE Asian winter monsoon linked to increasing insolation during this interval [*Wang et al.*, 2001] would have additionally enhanced the thermocline cooling trend (Figure 6). This effect even continued in the early part of HE 5, as the onset of ITF slowdown appears delayed during this HE.

[36] However, thermocline cooling stopped rather abruptly at the end of HE 5, and the intensity of the thermocline outflow remained overall decreased after HE 5 (Figure 3). After 47 ka, peak insolation over the neighboring Australian continent appears to have strongly influenced the hydrography of the Timor Sea (Figure 6). The sharp decrease in ITF intensity at the end of HE 5, which interrupts the long-term thermocline cooling trend from ~60 to 47 ka occurs ~1 ka before a prominent surface cooling at 46 ka, lasting until 40 ka. *Dürkop et al.* [2008] interpreted this event as the intrusion of a cold surface water tongue with increased influence of cooler, more nutrient rich waters from the West Australian Current and overall weakening of the ITF. The maximum in austral summer (21 December, 25°S) insolation at 47 ka would have favored the intensification of monsoonal winds over northern Australia, and in turn influenced the migration of hydrological fronts between Indian Ocean– and ITF-derived water masses, thus altering ITF flow and intensity.

5. Conclusion

[37] Our high-resolution stable isotope and Mg/Ca records of surface and thermocline dwelling planktonic foraminifers in core MD01-2378 from the Timor Sea indicate substantial temperature and salinity ($\delta^{18}O_{sw}$) changes in ITF outflow water masses during HEs 3–6. We interpret thermocline warming during HEs 3–6 as evidence for the increased influence of warmer, saltier thermocline water from the tropical Indian Ocean and attendant decrease in cool, fresh ITF thermocline flow, due to an overall slowdown in the global thermohaline circulation during HEs 3–6. These changes in the ITF structure and intensity during HEs must have had far-reaching repercussions on the hydrography of the tropical Indian Ocean as well as regional and global climate evolution. The resulting warmer and saltier eastern tropical Indian Ocean would have in turn strongly influenced the Asian Monsoon system and significantly altered the heat and energy budget within the "warm" return branch of the global thermohaline circulation.

[38] Three main factors appear to have influenced ITF variability during MIS 3: (1) global slowdown in thermohaline circulation during HEs, triggered by Northern Hemisphere cooling and restricted deep water formation in the North Atlantic; (2) increased freshwater export from the Java Sea into the ITF during the early part of MIS 3, principally controlled by sea level and (3) insolation-related changes in Australasian monsoonal intensity leading to the migration of hydrological fronts between Indian Ocean– and ITF-derived water masses at 46–40 ka. The complex interplay between these factors resulted in a unique pattern of ITF variability during MIS 3, which differs from changes recorded on glacial-interglacial timescales. Previous work focusing on Terminations I and II indicated that an overriding control of ITF thermocline flow intensity during terminations was the establishment of an open connection through the Java Sea to the South China Sea, when sea level

Figure 6. Comparison of sea level reconstructions, benthic $\delta^{18}O_{sw}$, temperatures, and insolation during MIS 3. (a) The 21 December maximum insolation at 25°S. (b) *P. obliquiloculata* Mg/Ca-derived upper thermocline temperature. (c) *G. ruber* (white) Mg/Ca-derived SST. (d) Benthic $\delta^{18}O_{sw}$: plus signs indicate tie points to sea level curve from the central Red Sea [*Siddall et al.*, 2003], and crosses indicate tie points to sea level curve from the northern Red Sea [*Arz et al.*, 2007]. (e) Sea level curve from the northern Red Sea [*Arz et al.*, 2007] tuned to MD01-2378 to maintain chronological consistency. (f) Coral-based sea level data from Huon Peninsula plotted on an independent age scale [*Chappell et al.*, 1996]. (g) Sea level curve from the central Red Sea [*Siddall et al.*, 2003] tuned to MD01-2378 to maintain chronological consistency. Thermocline cooling coincident with rising sea level (~60 m below present) and increasing insolation over Australia in the early part of MIS 3 (60–47 ka) is indicated by the gray bar.

reached ~40 m below present, in conjunction with a fully developed Australasian monsoonal system [*Xu et al.*, 2008]. Such conditions were only reached at peak interglacials during MIS 5e and the late Holocene.

[39] **Acknowledgments.** We thank Franck Bassinot, Yvon Balut, and the crew of the R/V *Marion Dufresne* for their efforts during the WEPAMA cruise and the Institut Polaire Français Paul Emile Victor for support. We are grateful to Gerald Dickens and two anonymous reviewers for in-depth, constructive reviews and to Jian Xu, Marcus Regenberg, and Andre Bahr for helpful comments. Dieter Garbe-Schönberg, Nadine Gehre, Karin Kissling, and Lulzim Haxhiaj provided analytical expertise and technical assistance. We gratefully acknowledge the Deutsche Forschungsgemeinschaft for funding this research (grant Ku 649/25) and the German Ministry for Education, Science and Technology (BMBF grant 03GO185B) for funding the Sonne 185 cruise.

References

Alley, R. B., and P. U. Clark (1999), The deglaciation of the Northern Hemisphere: A global perspective, *Annu. Rev. Earth Planet. Sci.*, *27*(1), 149–182, doi:10.1146/annurev.earth.27.1.149.

Anand, P., H. Elderfield, and M. H. Conte (2003), Calibration of Mg/Ca thermometry in planktonic foraminifera from a sediment trap time series, *Paleoceanography*, *18*(2), 1050, doi:10.1029/2002PA000846.

Andersen, K. K., et al. (2006), The Greenland ice core chronology 2005, 15–42 ka. Part 1: Constructing the time scale, *Quat. Sci. Rev.*, *25*(23–24), 3246–3257, doi:10.1016/j.quascirev.2006.08.002.

Antonov, J. I., R. A. Locarnini, T. P. Boyer, A. V. Mishonov, and H. E. Garcia (2006), *World Ocean Atlas 2005*, vol. 2, *Salinity*, *NOAA Atlas NESDIS*, vol. 62, edited by S. Levitus, 182 pp., NOAA, Silver Spring, Md.

Arz, H. W., F. Lamy, A. Ganopolski, N. Nowaczyk, and J. Pätzold (2007), Dominant Northern Hemisphere climate control over millennial-scale glacial sea-level variability, *Quat. Sci. Rev.*, *26*(3–4), 312–321, doi:10.1016/j.quascirev.2006.07.016.

Barker, S., M. Greaves, and H. Elderfield (2003), A study of cleaning procedures used for foraminiferal Mg/Ca paleothermometry, *Geochem. Geophys. Geosyst.*, *4*(9), 8407, doi:10.1029/2003GC000559.

Bé, A. W. H. (1977), An ecological, zoogeographical and taxonomic review of recent planktonic foraminifera, in *Oceanic Micropaleontology*, edited by A. T. S. Ramsay, pp. 1–100, Elsevier, New York.

Bemis, B. E., H. J. Spero, J. Bijma, and D. W. Lea (1998), Reevaluation of the oxygen isotopic composition of planktonic foraminifera: Experimental results and revised paleotemperature equations, *Paleoceanography*, *13*(2), 150–160, doi:10.1029/98PA00070.

Blunier, T., and E. J. Brook (2001), Timing of millennial-scale climate change in Antarctica and Greenland during the last glacial period, *Science*, *291*(5501), 109–112, doi:10.1126/science.291.5501.109.

Blunier, T., et al. (1998), Asynchrony of Antarctic and Greenland climate change during the last glacial period, *Nature*, *394*(6695), 739–743, doi:10.1038/29447.

Broecker, W. S. (1998), Paleocean circulation during the last deglaciation: A bipolar seesaw?, *Paleoceanography*, *13*(2), 119–121, doi:10.1029/97PA03707.

Broecker, W. S. (2003), Does the trigger for abrupt climate change reside in the ocean or in the atmosphere?, *Science*, *300*(5625), 1519–1522, doi:10.1126/science.1083797.

Cacho, I., J. O. Grimalt, C. Pelejero, M. Canals, F. J. Sierro, J. A. Flores, and N. Shackleton (1999), Dansgaard-Oeschger and Heinrich event imprints in Alboran Sea paleotemperatures, *Paleoceanography*, *14*(6), 698–705, doi:10.1029/1999PA900044.

Chappell, J., A. Omura, T. Esat, M. McCulloch, J. Pandolfi, Y. Ota, and B. Pillans (1996), Reconciliation of late Quaternary sea levels derived from coral terraces at Huon Peninsula with deep sea oxygen isotope records, *Earth Planet. Sci. Lett.*, *141*(1–4), 227–236.

Clark, P. U., S. W. Hostetler, N. G. Pisias, A. Schmittner, and K. J. Meissner (2007), Mechanisms for an ~7-kyr climate and sea-level oscillation during marine isotope stage 3, in *Ocean Circulation: Mechanisms and Impacts—Past and Future Changes of Meridional Overturning*, *Geophys. Monogr. Ser.*, vol. 173, edited by A. Schmittner, J. C. H. Chiang, and S. R. Hemming, pp. 209–246, AGU, Washington, D. C.

Cléroux, C., E. Cortijo, J.-C. Duplessy, and R. Zahn (2007), Deep-dwelling foraminifera as thermocline temperature recorders, *Geochem. Geophys. Geosyst.*, *8*, Q04N11, doi:10.1029/2006GC001474.

Dannenmann, S., B. K. Linsley, D. W. Oppo, Y. Rosenthal, and L. Beaufort (2003), East Asian monsoon forcing of suborbital variability in the Sulu Sea during marine isotope stage 3: Link to Northern Hemisphere climate, *Geochem. Geophys. Geosyst.*, *4*(1), 1001, doi:10.1029/2002GC000390.

De Deckker, P., N. J. Tapper, and S. van der Kaars (2003), The status of the Indo-Pacific warm pool and adjacent land at the Last Glacial Maximum, *Global Planet. Change*, *35*(1–2), 25–35, doi:10.1016/S0921-8181(02)00089-9.

Dürkop, A., A. Holbourn, W. Kuhnt, R. Zuraida, N. Andersen, and P. M. Grootes (2008), Centennial-scale climate variability in the Timor Sea during marine isotope stage 3, *Mar. Micropaleontol.*, *66*(3–4), 208–221, doi:10.1016/j.marmicro.2007.10.002.

Eggins, S., P. De Deckker, and J. Marshall (2003), Mg/Ca variation in planktonic foraminifera tests: Implications for reconstructing palaeo-seawater temperature and habitat migration, *Earth Planet. Sci. Lett.*, *212*(3–4), 291–306, doi:10.1016/S0012-821X(03)00283-8.

EPICA Community Members (2004), Eight glacial cycles from an Antarctic ice core, *Nature*, *429*(6992), 623–628, doi:10.1038/nature02599.

EPICA Community Members (2006), One-to-one coupling of glacial climate variability in Greenland and Antarctica, *Nature*, *444*(7116), 195–198, doi:10.1038/nature05301.

Erichsen, A. (2008), Impact of calcite dissolution on Mg/Ca ratios of core-top planktonic foraminifers from the Timor Sea, diploma thesis, 48 pp., Math.-Naturwiss. Fak., Christian-Albrechts-Univ. zu Kiel, Kiel, Germany.

Ganopolski, A., and S. Rahmstorf (2001), Rapid changes of glacial climate simulated in a coupled climate model, *Nature*, *409*(6817), 153–158, doi:10.1038/35051500.

Gordon, A. L. (2005), Oceanography of the Indonesian Seas and their throughflow, *Oceanography*, *18*(4), 14–27.

Gordon, A. L., R. D. Susanto, and K. Vranes (2003), Cool Indonesian Throughflow as a consequence of restricted surface layer flow, *Nature*, *425*(6960), 824–828, doi:10.1038/nature02038.

Hemleben, C., M. Spindler, and O. R. Anderson (1989), *Modern Planktonic Foraminifera*, 363 pp., Springer, New York.

Hemming, S. R. (2004), Heinrich events: Massive late Pleistocene detritus layers of the North Atlantic and their global climate imprint, *Rev. Geophys.*, *42*, RG1005, doi:10.1029/2003RG000128.

Hendy, I. L., and J. P. Kennett (2000), Dansgaard-Oeschger cycles and the California Current System: Planktonic foraminiferal response to rapid climate change in Santa Barbara Basin, Ocean Drilling Program Hole 893A, *Paleoceanography*, *15*(1), 30–42, doi:10.1029/1999PA000413.

Holbourn, A., W. Kuhnt, H. Kawamura, Z. Jian, P. Grootes, H. Erlenkeuser, and J. Xu (2005), Orbitally paced paleoproductivity variations in the Timor Sea and Indonesian Throughflow variability during the last 460 kyr, *Paleoceanography*, *20*, PA3002, doi:10.1029/2004PA001094.

Huber, C., M. Leuenberger, R. Spahni, J. Flückiger, J. Schwander, T. F. Stocker, S. Johnsen, A. Landais, and J. Jouzel (2006), Isotope calibrated Greenland temperature record over marine isotope stage 3 and its relation to CH_4, *Earth Planet. Sci. Lett.*, *243*(3–4), 504–519, doi:10.1016/j.epsl.2006.01.002.

Ilahude, A. G., and A. L. Gordon (1996), Thermocline stratification within the Indonesian Seas, *J. Geophys. Res.*, *101*(C5), 12,401–12,409, doi:10.1029/95JC03798.

Kuhnt, W., et al. (2006), Cruise report SONNE-185—Variability of the Indonesian Throughflow and Australasian climate history of the last 150 000 years (VITAL), report, Inst. für Geowiss., Christian-Albrechts-Univ. zu Kiel, Kiel, Germany.

Labeyrie, L. D., J. C. Duplessy, and P. L. Blanc (1987), Variations in mode of formation and temperature of oceanic deep waters over the past 125,000 years, *Nature*, *327*(6122), 477–482, doi:10.1038/327477a0.

Levi, C., L. Labeyrie, F. Bassinot, F. Guichard, E. Cortijo, C. Waelbroeck, N. Caillon, J. Duprat, T. de Garidel-Thoron, and H. Elderfield (2007), Low-latitude hydrological cycle and rapid climate changes during the last deglaciation, *Geochem. Geophys. Geosyst.*, *8*, Q05N12, doi:10.1029/2006GC001514.

Lin, H.-L., L. C. Peterson, J. T. Overpeck, S. E. Trumbore, and D. W. Murray (1997), Late Quaternary climate change from $\delta^{18}O$ records of multiple species of planktonic foraminifera: High-resolution records from the anoxic Cariaco Basin, Venezuela, *Paleoceanography*, *12*(3), 415–427, doi:10.1029/97PA00230.

Locarnini, R. A., A. V. Mishonov, J. I. Antonov, T. P. Boyer, and H. E. Garcia (2006), *World*

Ocean Atlas 2005, vol. 1, *Temperature*, *NOAA Atlas NESDIS*, vol. 61, edited by S. Levitus, 182 pp., NOAA, Silver Spring, Md.

Lynch-Stieglitz, J. (2004), Ocean science: Hemispheric asynchrony of abrupt climate change, *Science*, *304*(5679), 1919–1920, doi:10.1126/science.1100374.

Muller, J., M. Kylander, R. A. J. Wüst, D. Weiss, A. Martinez-Cortizas, A. N. LeGrande, T. Jennerjahn, H. Behling, W. T. Anderson, and G. Jacobson (2008), Possible evidence for wet Heinrich phases in tropical NE Australia: The Lynch's Crater deposit, *Quat. Sci. Rev.*, *27*(5–6), 468–475, doi:10.1016/j.quascirev.2007.11.006.

Murgese, D. S., and P. De Deckker (2007), The late Quaternary evolution of water masses in the eastern Indian Ocean between Australia and Indonesia, based on benthic foraminifera faunal and carbon isotopes analyses, *Palaeogeogr. Palaeoclimatol. Palaeoecol.*, *247*, 382–401, doi:10.1016/j.palaeo.2006.11.002.

Pahnke, K., and R. Zahn (2005), Southern Hemisphere water mass conversion linked with North Atlantic climate variability, *Science*, *307*(5716), 1741–1746, doi:10.1126/science.1102163.

Partin, J. W., K. M. Cobb, J. F. Adkins, B. Clark, and D. P. Fernandez (2007), Millennial-scale trends in West Pacific Warm Pool hydrology since the Last Glacial Maximum, *Nature*, *449*(7161), 452–455, doi:10.1038/nature06164.

Pflaumann, U., and Z. Jian (1999), Modern distribution patterns of planktonic foraminifera in the South China Sea and western Pacific: A new transfer technique to estimate regional sea-surface temperatures, *Mar. Geol.*, *156*(1–4), 41–83, doi:10.1016/S0025-3227(98)00173-X.

Piotrowski, A. M., S. L. Goldstein, S. R. Hemming, and R. G. Fairbanks (2004), Intensification and variability of ocean thermohaline circulation through the last deglaciation, *Earth Planet. Sci. Lett.*, *225*(1–2), 205–220, doi:10.1016/j.epsl.2004.06.002.

Piotrowski, A. M., S. L. Goldstein, S. R. Hemming, and R. G. Fairbanks (2005), Temporal relationships of carbon cycling and ocean circulation at glacial boundaries, *Science*, *307*(5717), 1933–1938, doi:10.1126/science.1104883.

Prell, W. L., and J. E. Damuth (1978), The climate-related diachronous disappearance of *Pulleniatina obliquiloculata* in late Quaternary sediments of the Atlantic and Caribbean, *Mar. Micropaleontol.*, *3*(3), 267–277, doi:10.1016/0377-8398(78)90031-2.

Ravelo, A. C., and R. G. Fairbanks (1992), Oxygen isotopic composition of multiple species of planktonic foraminifera: Recorders of the modern photic zone temperature gradient, *Paleoceanography*, *7*(6), 815–831, doi:10.1029/92PA02092.

Ravelo, A. C., R. G. Fairbanks, and S. G. H. Philander (1990), Reconstructing tropical Atlantic hydrography using planktonic foraminifera and an ocean model, *Paleoceanography*, *5*(3), 409–431, doi:10.1029/PA005i003p00409.

Rohling, E. J. (2007), Progress in paleosalinity: Overview and presentation of a new approach, *Paleoceanography*, *22*, PA3215, doi:10.1029/2007PA001437.

Rosenthal, Y., D. W. Oppo, and B. K. Linsley (2003), The amplitude and phasing of climate change during the last deglaciation in the Sulu Sea, western equatorial Pacific, *Geophys. Res. Lett.*, *30*(8), 1428, doi:10.1029/2002GL016612.

Sarnthein, M., K. Winn, S. J. A. Jung, J.-C. Duplessy, L. Labeyrie, H. Erlenkeuser, and G. Ganssen (1994), Changes in East Atlantic deepwater circulation over the last 30,000 years: Eight time slice reconstructions, *Paleoceanography*, *9*(2), 209–267, doi:10.1029/93PA03301.

Sarnthein, M., et al. (2001), Fundamental modes and abrupt changes in North Atlantic circulation and climate over the last 60 ky—Concepts, reconstruction and numerical modeling, in *The Northern North Atlantic: A Changing Environment*, edited by P. Schäfer et al., pp. 365–410, Springer, Berlin.

Shackleton, N. J. (1987), Oxygen isotopes, ice volume and sea level, *Quat. Sci. Rev.*, *6*(3–4), 183–190, doi:10.1016/0277-3791(87)90003-5.

Shackleton, N. J., M. A. Hall, and E. Vincent (2000), Phase relationships between millennial-scale events 64,000–24,000 years ago, *Paleoceanography*, *15*(6), 565–569, doi:10.1029/2000PA000513.

Siddall, M., E. J. Rohling, A. Almogi-Labin, C. Hemleben, D. Meischner, I. Schmelzer, and D. A. Smeed (2003), Sea-level fluctuations during the last glacial cycle, *Nature*, *423*(6942), 853–858, doi:10.1038/nature01690.

Spooner, M. I., T. T. Barrows, P. De Deckker, and M. Paterne (2005), Palaeoceanography of the Banda Sea, and late Pleistocene initiation of the northwest monsoon, *Global Planet. Change*, *49*(1–2), 28–46, doi:10.1016/j.gloplacha.2005.05.002.

Sprintall, J., J. T. Potemra, S. L. Hautala, N. A. Bray, and W. W. Pandoe (2003), Temperature and salinity variability in the exit passages of the Indonesian Throughflow, *Deep Sea Res., Part II*, *50*(12–13), 2183–2204, doi:10.1016/S0967-0645(03)00052-3.

Stott, L., C. Poulsen, S. Lund, and R. Thunell (2002), Super ENSO and global climate oscillations at millennial time scales, *Science*, *297*(5579), 222–226, doi:10.1126/science.1071627.

Suppiah, R., and X. Wu (1998), Surges, cross-equatorial flows and their links with the Australian summer monsoon circulation and rainfall, *Aust. Meteorol. Mag.*, *47*(2), 113–130.

Svensson, A., et al. (2006), The Greenland ice core chronology 2005, 15–42 ka. Part 2: Comparison to other records, *Quat. Sci. Rev.*, *25*(23–24), 3258–3267, doi:10.1016/j.quascirev.2006.08.003.

Svensson, A., et al. (2008), A 60 000 year Greenland stratigraphic ice core chronology, *Clim. Past*, *4*, 47–57.

Tedesco, K. A., and R. C. Thunell (2003), Seasonal and interannual variations in planktonic foraminiferal flux and assemblage composition in the Cariaco Basin, Venezuela, *J. Foraminiferal Res.*, *33*(3), 192–210, doi:10.2113/33.3.192.

Wang, X., A. S. Auler, R. L. Edwards, H. Cheng, P. S. Cristalli, P. L. Smart, D. A. Richards, and C.-C. Shen (2004), Wet periods in northeastern Brazil over the past 210-kyr linked to distant climate anomalies, *Nature*, *432*(7018), 740–743, doi:10.1038/nature03067.

Wang, Y. J., H. Cheng, R. L. Edwards, Z. S. An, J. Y. Wu, C.-C. Shen, and J. A. Dorale (2001), A high-resolution absolute-dated late Pleistocene monsoon record from Hulu Cave, China, *Science*, *294*(5550), 2345–2348, doi:10.1126/science.1064618.

Xu, J., W. Kuhnt, A. Holbourn, N. Andersen, and G. Bartoli (2006), Changes in the vertical profile of the Indonesian Throughflow during Termination II: Evidence from the Timor Sea, *Paleoceanography*, *21*, PA4202, doi:10.1029/2006PA001278.

Xu, J., A. Holbourn, W. Kuhnt, Z. Jian, and H. Kawamura (2008), Changes in the thermocline structure of the Indonesian outflow during terminations I and II, *Earth Planet. Sci. Lett.*, *273*(1–2), 152–162, doi:10.1016/j.epsl.2008.06.029.

A. Dürkop, A. Erichsen, A. Holbourn, W. Kuhnt, and R. Zuraida, Institute of Geosciences, Christian Albrechts University, Ludewig-Meyn-Strasse 10-14, D-24118 Kiel, Germany.

D. Nürnberg, Leibniz Institute of Marine Sciences at University of Kiel (IFM-GEOMAR), Wischhofstrasse 1-3, D-24148 Kiel, Germany. (rzuraida@ifm-geomar.de)